

## Article

# Synthesis of Zinc Oxide Nanomaterials via Sol-Gel Process with Anti-Corrosive Effect for Cu, Al and Zn Metallic Substrates

Raluca Somoghi <sup>1</sup>, Violeta Purcar <sup>1,\*</sup>, Elvira Alexandrescu <sup>1</sup>, Ioana Catalina Gifu <sup>1</sup>,  
Claudia Mihaela Ninciuleanu <sup>1</sup>, Cosmin Mihai Cotrut <sup>2</sup>, Florin Oancea <sup>1</sup> and Hermine Stroescu <sup>3</sup>

<sup>1</sup> National Institute for Research & Development in Chemistry and Petrochemistry-ICECHIM Bucharest, 202 Splaiul Independentei, 6th District, 060021 Bucharest, Romania; r.somoghi@gmail.com (R.S.); elviraalexandrescu@yahoo.com (E.A.); gifu\_ioanacatalina@yahoo.com (I.C.G.); claudia.ninciuleanu@yahoo.com (C.M.N.); florin.oancea@icechim.ro (F.O.)

<sup>2</sup> Department of Metallic Materials Science, Physical Metallurgy, Faculty of Material Science and Engineering, University Politehnica of Bucharest, 313 Splaiul Independentei Street, Building J, 060042 Bucharest, Romania; cosmin.cotrut@upb.ro

<sup>3</sup> Institute of Physical Chemistry "Ilie Murgulescu" of the Romanian Academy, 202 Splaiul Independentei, 6th District, 060021 Bucharest, Romania; hstroescu@icf.ro

\* Correspondence: purcarvioleta@gmail.com

**Abstract:** Nanosized zinc oxide (ZnO) particles modified with different silane coupling agents (octyltriethoxysilane (OTES), octadecyltriethoxysilane (ODTES) and (3-glycidylxypropyl)trimethoxysilane (GPTMS)) were synthesized in basic catalysis using the sol-gel method. The structure and morphology were characterized by dynamic light scattering (DLS), environmental scanning electron microscopy (ESEM) and Fourier transform infrared spectroscopy (FTIR) for bonding characteristics. The final hybrid materials were deposited on three types of metallic substrates (aluminum (Al), copper (Cu) and zinc (Zn)) in order to obtain coatings with ultrahydrophobic and anti-corrosion properties. Water wettability was studied revealing a contact angle of 145° for the surface covered with ZnO material modified with ODTES. The water contact angle increased with the length of the alkyl chain supplied by the silica precursor. The anti-corrosive behavior of ZnO/silane coupling agents particles deposited on metallic substrates was studied by the linear polarization technique in neutral medium.

**Keywords:** ZnO nanoparticles; sol-gel; metallic substrates



**Citation:** Somoghi, R.; Purcar, V.; Alexandrescu, E.; Gifu, I.C.; Ninciuleanu, C.M.; Cotrut, C.M.; Oancea, F.; Stroescu, H. Synthesis of Zinc Oxide Nanomaterials via Sol-Gel Process with Anti-Corrosive Effect for Cu, Al and Zn Metallic Substrates. *Coatings* **2021**, *11*, 444. <https://doi.org/10.3390/coatings11040444>

Academic Editor: Aomar Hadjadj

Received: 22 February 2021

Accepted: 9 April 2021

Published: 13 April 2021

**Publisher's Note:** MDPI stays neutral with regard to jurisdictional claims in published maps and institutional affiliations.



**Copyright:** © 2021 by the authors. Licensee MDPI, Basel, Switzerland. This article is an open access article distributed under the terms and conditions of the Creative Commons Attribution (CC BY) license (<https://creativecommons.org/licenses/by/4.0/>).

## 1. Introduction

Zinc oxide nanoparticles (ZnO-NPs) are obtained from the most commonly used metal oxide for obtaining nanomaterials according to Faizan, with a global annual production estimate to be between 550 and 33,400 tons [1,2]. This is mainly due to the diversified morphology and excellent physicochemical properties of these nanoparticles [3,4], with a spectrum of possible applications in surface coatings, sensors, photoelectric material, medicine, anti-bacterial, anti-fungal, anti-fouling, anti-aging, UV blocking agents, solar filters, transistors, acoustic devices, optoelectronics, aircraft nanocoatings, zinc-rich paints and many other fields [3,5–9]. ZnO nanoparticles are mostly known for their low cost, low environmental impact and excellent photoelectric performance.

With respect to the value of the water contact angle (WCA), we have four different regimes of surface wetting behavior [10]. Superhydrophobicity is described by WCAs of  $\theta > 150^\circ$ , which is a state of nearly perfect non-wetting. A variety of important properties have been incorporated in superhydrophobic surfaces such as water repellency and self-cleaning, transparency and color, anisotropy, reversibility, flexibility and breathability (moisture vapor transfer) [11].

The corrosive behavior in NaCl solution of superhydrophobic surfaces was investigated by Ou et al., after they prepared 1H, 1H, 2H, 2H-perfluorooctyltrichlorosilane (PFOTS) chemically adsorbed onto the etched titanium substrate [12]. They showed that

the final material had a higher stability and corrosion inhibition efficiency, due to the strong chemical interfacial bonding between PFOTS and Ti. Another group of researchers also synthesized a stable superhydrophobic film by myristic acid chemically adsorbed onto an anodized aluminum substrate. The contact angle was around  $154^\circ$ , and corrosion in seawater was significantly decreased [13].

Wu et al. fabricated a superhydrophobic coating on the surface of poplar wood, with a contact angle of up to  $158.4^\circ$  through the water-based UV-cured wood coating which was modified by ZnO and stearic acid. The results showed that under acidic conditions, the nonpolar long alkyl chain group of the stearic acid molecule reacted with the hydroxyl group in acetic acid, the metal ions of the ZnO were displaced to the stearic acid and generated globular zinc stearate ( $C_{36}H_{70}O_4Zn$ ) [4].

One of the most commonly used methods for corrosion protection based on sol-gel technology is the design of hydrophobic or super-hydrophobic surfaces, because of their ability to repel water and aqueous electrolyte, anti-icing and anti-fouling [10,14]. In this respect, a very good strategy is to change the morphology of the outer surface of the sol-gel coating by using silane coupling agents with different alkyl chains. The new trends are based on the use of sol-gel coatings modified with inorganic nanoparticles with the aim of obtaining a better mechanical resistance.

The sol-gel approach appears to be one of the most promising methods to prepare ZnO nanoparticles for several reasons: the ease of synthesis, low temperature of decomposition, control over the chemical composition, low cost, reliability, repeatability and relatively mild synthesis conditions [15–17]. In general, the most effective corrosion protection systems were based on the use of chromate-rich surface treatments, which are prohibited by the current legislation in almost all sectors. Consequently, alternatives were developed, including a high number of “green” surface treatments, environmentally safe pigments and natural corrosion inhibitors. Corrosion is a destructive phenomenon, very difficult to avoid but easily controlled via metal dissolution, which reduces the corrosion rate through various mechanisms, such as metal coating, cathodic protection process and inhibition [18–22]. In the last two decades, the potential of organofunctional silane coatings for the replacement of chrome conversion treatments has been the topic of a number of important studies [14]. El-Nahhal et al. [23] demonstrates that the silica coated ZnO composites, functionalized using alkoxysilanes with amine or thiol organofunctional groups, can be used for the removal of heavy metals.

Related to corrosion, some studies were made on these materials proving their potential use as adhesion promoters between metallic substrates and organic coatings. The role of silane films is to provide adhesion between metal substrates and organic coatings while forming a thin but efficient barrier against the diffusion of oxygen to the metal interface [15]. This study presented two ways of ZnO functionalization with metal: in situ growth of NPs on the desired ZnO nanostructure or adsorption of pre-synthesized NPs [24]. Adsorption of pre-synthesized NPs was shown to be a better choice due to the advantages of a fully controlled NP synthesis method. Aluminum (Al) is a reactive metal in the galvanic series, but in contact with other metals, it will act as the anode and may begin to corrode [25]. Though the passive oxide on aluminum is relatively protective against corrosion, corrosion of aluminum alloys always occurs locally because of the presence of intermetallic second phase particles [26]. Copper (Cu) is one of the most versatile engineering materials developed to date. It is used in different industries due to its thermal and electrical conductivity, corrosion resistance and reasonable mechanical properties. However, copper is vulnerable to corrosion and forms oxide films of different types depending on the nature of the environment it is exposed to, requiring further protection by coatings. Many different approaches, including coating with organic or inorganic layers have been developed in order to protect copper from corrosion [27,28]. Many studies have been conducted on the corrosive behavior of zinc (Zn) in various types of atmosphere. It was found that the high corrosion resistance of zinc is due to the formation of corrosion products on its surface [29]. Much research has been carried out for optimization of the zinc coating composition by

alloy, in order to improve long-term corrosion stability and reduce costs of zinc coated steel products [30,31].

In this work, ZnO nanoparticles were modified through sol-gel method with octyltriethoxysilane (OTES), (3-glycidyloxypropyl)trimethoxysilane (GPTMS) and octadecyltriethoxysilane (ODTES) coupling agents, in order to improve the anti-corrosive properties of three metallic substrates: aluminum (Al), copper (Cu) and zinc. (Zn) The water contact angles of the final metallic coatings were measured and their corrosion behavior was investigated through linear polarization technique. The dynamic light scattering (DLS), environmental scanning electron microscopy (ESEM) and Fourier transform infrared spectroscopy (FTIR) analyses were useful to characterize the synthesized materials and to correlate the results with the structural and morphological properties of the final materials. The wetting capacity of the coatings was determined through contact angle (CA) measurements with water as the wetting agent. CA is a measure of the adhesion between liquid drops (water) and the solid surface. The final aim was to modify ZnO powder with silane functional groups able to change the ZnO material surface from a hydrophilic to a hydrophobic nature. The obtained zinc oxide nanomaterials produced in this way can be extended to many industrial applications due to the good electrical and optical properties, especially in the electronic industry.

## 2. Materials and Methods

All the chemical reagents and solvents were commercially purchased and used without further purification. Commercial ZnO nanopowder (<100 nm, ZnO, Sigma-Aldrich, Philadelphia, PA, USA), tetraethoxysilane (TEOS, 98%, Sigma-Aldrich, Philadelphia, PA, USA), octyltriethoxysilane (OTES, 97.5%, Sigma-Aldrich, Philadelphia, PA, USA), octadecyltriethoxysilane (ODTES, 98%, Alfa Aesar, Karlsruhe, Germany), (3-glycidyloxypropyl)trimethoxysilane (GPTMS, 97%, Fluka, Philadelphia, PA, USA), ammonium hydroxide solution (NH<sub>4</sub>OH, 32%, Sigma-Aldrich, Philadelphia, PA, USA), ethanol (EtOH, 99.9%, Chimreactiv S.R.L., Bucharest, Romania), 2-propanol (99.9%, Chimreactiv S.R.L., Bucharest, Romania) and demineralized water were used in this study.

Three types of metallic substrates (aluminum (99.99%, Shanghai, China), copper (99.99%, Sibiu, Romania) and zinc (99%, Galati, Romania)) were used in order to test the corrosion of coatings covered with ZnO materials.

### 2.1. Synthesis of Modified ZnO-Nanoparticles

A typical experiment for the preparation of zinc oxide nanomaterials was conducted at room temperature (25 °C) according to the following procedure adapted from literature [26–28]:

A small quantity of commercial ZnO nanopowder was homogeneously dispersed in a mixture of ethanol, demineralized water and ammonium hydroxide solution (32%) in an ultrasonication bath for one hour.

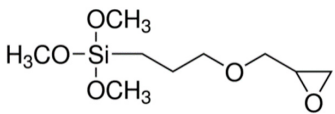
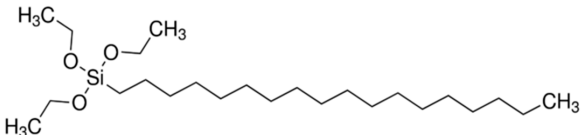
The homogenized solution was split into equal quantities in three vessels. In each vessel, we added the TEOS, in small droplets, and one of the three coupling agents (Table 1), with a molar ratio of TEOS/OTES (GPTMS; ODTES) = 1/1.

The final solutions were magnetically stirred for 6 h, 300 rpm, at room temperature (25 °C).

**Table 1.** Silane precursors and their chemical formulae.

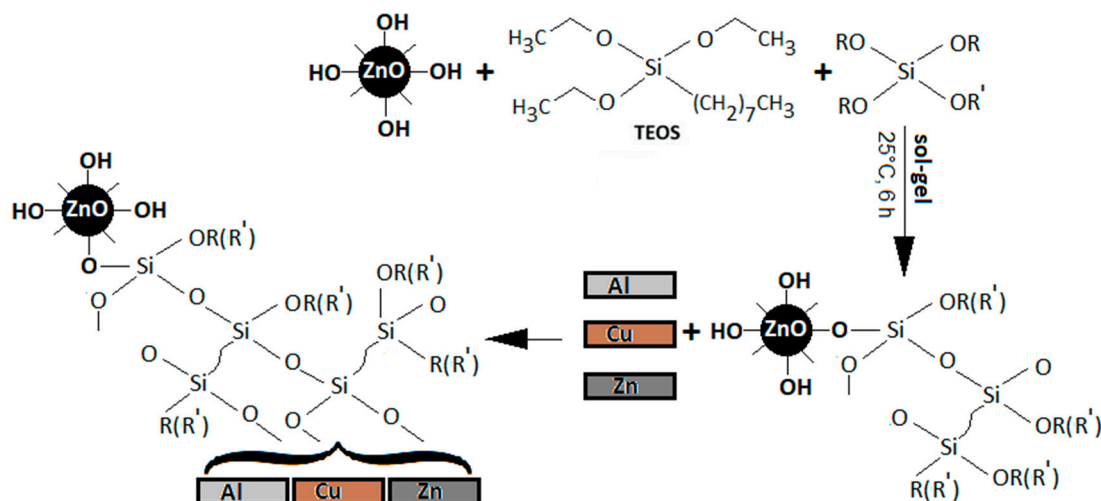
Sample No.	Silane Precursors		Chemical Formula
N1	Octyltriethoxysilane	OTES	$\text{H}_3\text{C}-\text{O}-\text{Si}(\text{O}-\text{CH}_3)_2-\text{CH}_2(\text{CH}_2)_6\text{CH}_3$

Table 1. Cont.

Sample No.	Silane Precursors		Chemical Formula
N2	(3-glycidyloxypropyl)trimethoxysilane	GPTMS	
N3	Octadecyltriethoxysilane	ODTES	

## 2.2. Metallic Coatings

The metallic substrates (aluminum (Al), copper (Cu) and zinc (Zn)) were cut into  $1 \times 1 \text{ cm}^2$  pieces, rubbed with sandpaper, rinsed with ethyl alcohol and dried under a hot air stream. Each piece of Zn, Cu and Al, was directly immersed in the final modified ZnO solutions 3 times, allowing them to dry exposed to the ambient air after each immersion (Scheme 1).



**Scheme 1.** Possible mechanism of the chemical reactions, R-CH<sub>3</sub>/C<sub>2</sub>H<sub>5</sub>, R<sup>1</sup>-octyl, octadecyl and 3-glycidyloxypropyl.

## 2.3. Characterization Methods

### 2.3.1. Dynamic Light Scattering Measurements

The particle sizes of ZnO modified with silane precursors were measured after their dilution (0.1 mL sample diluted in 25 mL 2-propanol) and ultrasonication for 5 min at room temperature (25 °C), using a ZetasizerNanoZS instrument (Malvern Instruments Ltd., Malvern, UK).

### 2.3.2. SEM Microscopy

Morphology and shape of the resulting modified silica ZnO particles were studied via environmental scanning electron microscopy (ESEM) using an FEI-Quanta 200 microscope (Phillips, The Netherlands).

### 2.3.3. FTIR Analysis

A Spectrometer Tensor 37 (Bruker Instrument, Woodstock, NY, USA), in ATR (Attenuated total reflection) mode with a Golden Gate diamond unite (400–4000 cm<sup>-1</sup>), was used

to examine the chemical bonds of the dried modified ZnO materials deposited on metallic substrates (Al, Cu and Zn).

#### 2.3.4. Contact Angle Measurement

A contact angle meter drop shape analysis system, model DSA1 (FM40 Easy Drop, DIP-ROBOT DR-3, Riegler and Kirstein, Berlin, Germany) was used for the evaluation of coatings' wettability. The static contact angle of deionized water on deposited films was obtained by analyzing the captured images using the tangent method algorithm at room temperature. An average value of the contact angle between the sample surfaces and a minimum of five deionized water drops was measured using the sessile drop method. The reported contact angle values were obtained as the average of five measurements (liquid droplets placed in various regions of the film surface).

#### 2.3.5. Electrochemical Characterization

Polarization resistance technique in the range of  $\pm 200$  mV vs. OCP (open circuit potential) with a scan rate of 1 mV/s was used to evaluate the corrosion kinetics of the coating systems (Tafel plots). The open circuit potential was monitored for one hour initially.

Electrochemical tests were performed using a Potentiostat/Galvanostat (PARSTAT 4000, Princeton Applied Research – Ametek, Oak Ridge, TN, USA), and Tafel curves were acquired with VersaStudio software version 2.52.3.

An electrochemical cell with a saturated calomel electrode (SCE)-reference electrode (RE), a platinum electrode-auxiliary electrode (AE) and the working electrode (WE)-coated metals samples, was employed to ascertain the electrochemical behavior. All tests were carried out in a 3.5% NaCl solution (saline solution—SS) at the temperature of  $25 \pm 0.5$  °C.

#### 2.3.6. Spectroscopic Ellipsometry (SE)

SE measurements were performed at room temperature on a VASE equipment (J.A. Woollam, Lincoln, NE, USA), in the spectral range of 400–1200 nm, with a 10 nm step resolution at 65° incident angle. The commercially available WVASE32 software package version 3.920 was used for the ellipsometric data simulation in order to determine the thickness and the roughness of the ZnO-based surface coatings deposited on three types of metallic substrates.

### 3. Results and Discussion

#### 3.1. DLS Measurements

DLS measurements were carried out on sol samples, immediately after synthesis, and before deposition on metallic substrates. The average nanoparticles sizes ( $D_m$ ) for the synthesized samples (diluted in solvent and ultrasonicated in a bath for 5 min), are presented in Figure 1. The particles' size values corresponding to the main and second populations of particles, and the polydispersity index PdI are shown in Table 2.

**Table 2.** Average sizes of main population (P1), second population (P2) of unmodified ZnO and modified ZnO-NPs (nanoparticles) with the specified types of alkoxy silanes ((TEOS/OTES), (TEOS/GPTMS), (TEOS/ODTES)) and the polydispersity index (PdI).

Alkoxy silane Type	Sample No.	Z Average (nm)	P1 (nm)	P2 (nm)	PdI
-	ZnO	299	268	-	0.291
TEOS/OTES	N1	437	352	87	0.641
TEOS/GPTMS	N2	269	226	-	0.313
TEOS/ODTES	N3	387	404	32	0.573

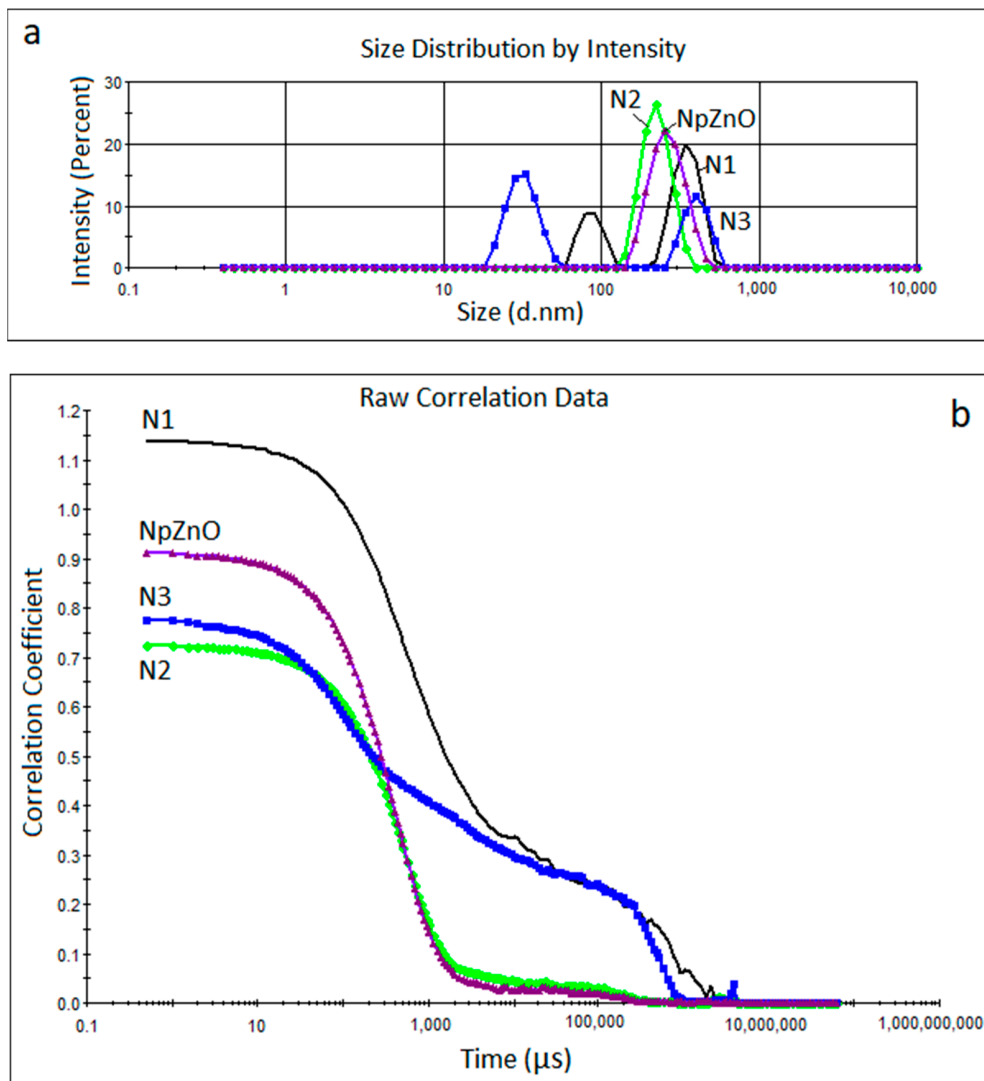


**Figure 1.** (a) Size distribution by intensity and (b) correlation coefficient for unmodified ZnO dispersion and for modified ZnO dispersions: N1 (ZnO-TEOS/OTES), N2 (ZnO-TEOS/GPTMS), N3 (ZnO-TEOS/ODTES).

For all the samples subjected to DLS analysis, the main populations of particles (P1) are assigned to pristine ZnO particles and, respectively, to the ZnO particles coated by different organic functions. The size of functionalized particles varies in the following order:  $N2 < N1 < N3$ , according to the length of the organic chains of the silanic precursor used to functionalize the ZnO particles: glycidyoxypropyl < octyl < octadecyl.

The size distribution by intensity curve of the reference sample (the pristine ZnO NPs) shows a monomodal size distribution, but the row correlation data diagram indicates the presence of some aggregates.

The alkyl-modified ZnO particles (samples N1 and N3) present variable dimensions, indicated by the high values of the polydispersity index ( $PdIN1 = 0.641$  and  $PdIN3 = 0.573$ ). Thus, for samples N1 and N3, a bimodal size distribution was recorded, as shown by the size distribution by intensity diagrams (Figure 1a), and also confirmed by the raw correlation data curves (Figure 1b).

Sample N2 has a monomodal size distribution, similar to the one recorded for the pristine ZnO NPs, and shows a narrower peak for particles size and a lower value of the polydispersity index than samples N1 and N3. It can be assumed that the silica precursors (GPTMS and TEOS) were efficiently coated on the ZnO particles surface, and no separation of unreacted species occurred. The average hydrodynamic diameter measured for P1 of sample N2 has a smaller value even when compared with the average hydrodynamic

diameter measured for P1 of the pristine ZnO nanoparticles. This can be explained by the stabilizing effect that the glycidyl functions may have, preventing aggregation of the glycidyl-modified ZnO particles.

The second population of particles (P2) recorded for samples N1 and N3, with average sizes smaller than 100 nm, is probably due to the generation of molecular assemblies between the unattached alkoxy silane derivatives on the ZnO nanoparticles surfaces. The hydrolysis and condensation reactions of the organic functions depend on the length of the alkyl chains. Thus, when compared with OTES, for the sample with ODTES coated particles, a higher fraction of the silica co-precursor remains unattached to the ZnO surface and separates.

### 3.2. Morphological Structure

The synthesized nanomaterials based on ZnO through sol-gel method and with different silane coupling agents were scanning electron microscopy (SEM) characterized as sol dispersions. Sample deposition was made immediately after synthesis, on the stub surface covered with aluminum tape. The phenomenon of particle aggregation took place after drying, which also favored the bonding together of particles as a result of the continuation of the sol-gel process.

Figure 2 shows ZnO-TEOS/OTES, ZnO-TEOS/GPTMS and ZnO-TEOS/ODTES with some morphological differences between all three samples [32]. Due to the microscope limits of detection, in SEM images only particles' aggregates can be observed, while the main population of particles detected in DLS could not be evidenced. The highest aggregation degree is exhibited by sample N3, with the longest organic function. Furthermore, ZnO nanoparticles are covered to a higher extent by the organic component (octadecyl). The smallest particle sizes can be noticed for sample N2, which was also confirmed by the DLS measurements.

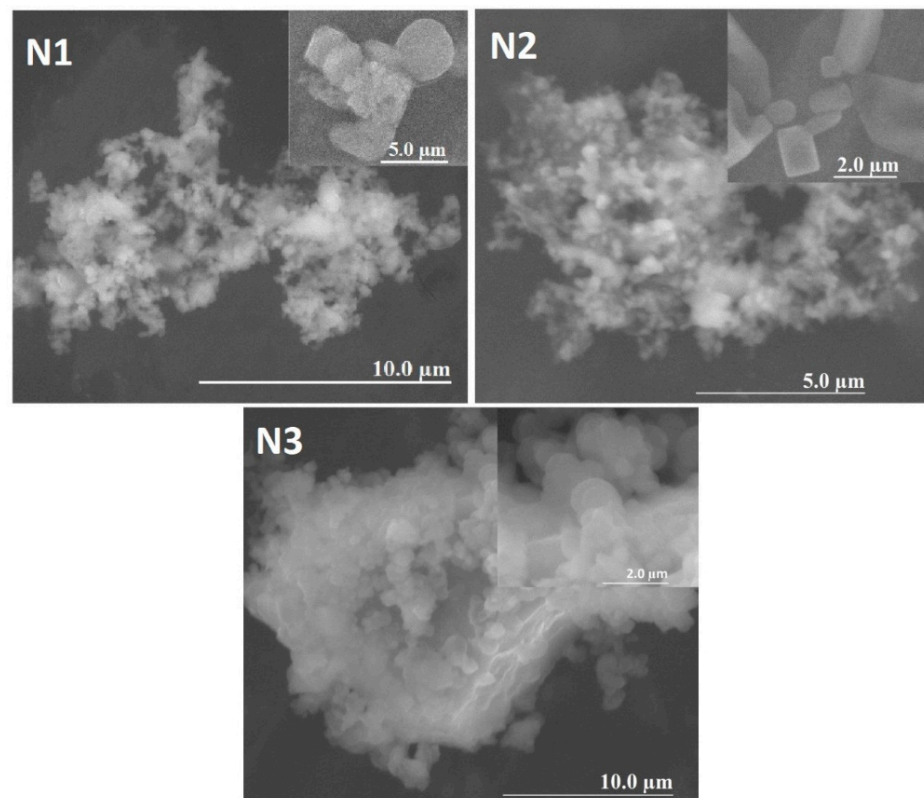


**Figure 2.** ESEM images of the surface of the ZnO materials modified with silanic precursors N1 (TEOS/OTES), N2 (TEOS/GPTMS), N3 (TEOS/ODTES).

### 3.3. FTIR Analysis

The typical FTIR spectra of uncoated substrates (Al, Cu, Zn) are shown in Figure 3a,c. The peak observed at  $2926\text{ cm}^{-1}$  is ascribed to symmetric stretching vibrations of  $\text{CH}_2$  groups [33]. Other peaks for the metals located at  $\sim 1450\text{ cm}^{-1}$  for symmetric vs. (COO) stretching vibrations can be seen as well [33,34]. The intense peak at  $1365\text{ cm}^{-1}$  can be attributed to the CH or  $\text{CH}_2$  bending modes [35]. A large carbonyl peak situated at  $\sim 1740\text{ cm}^{-1}$  was also observed.

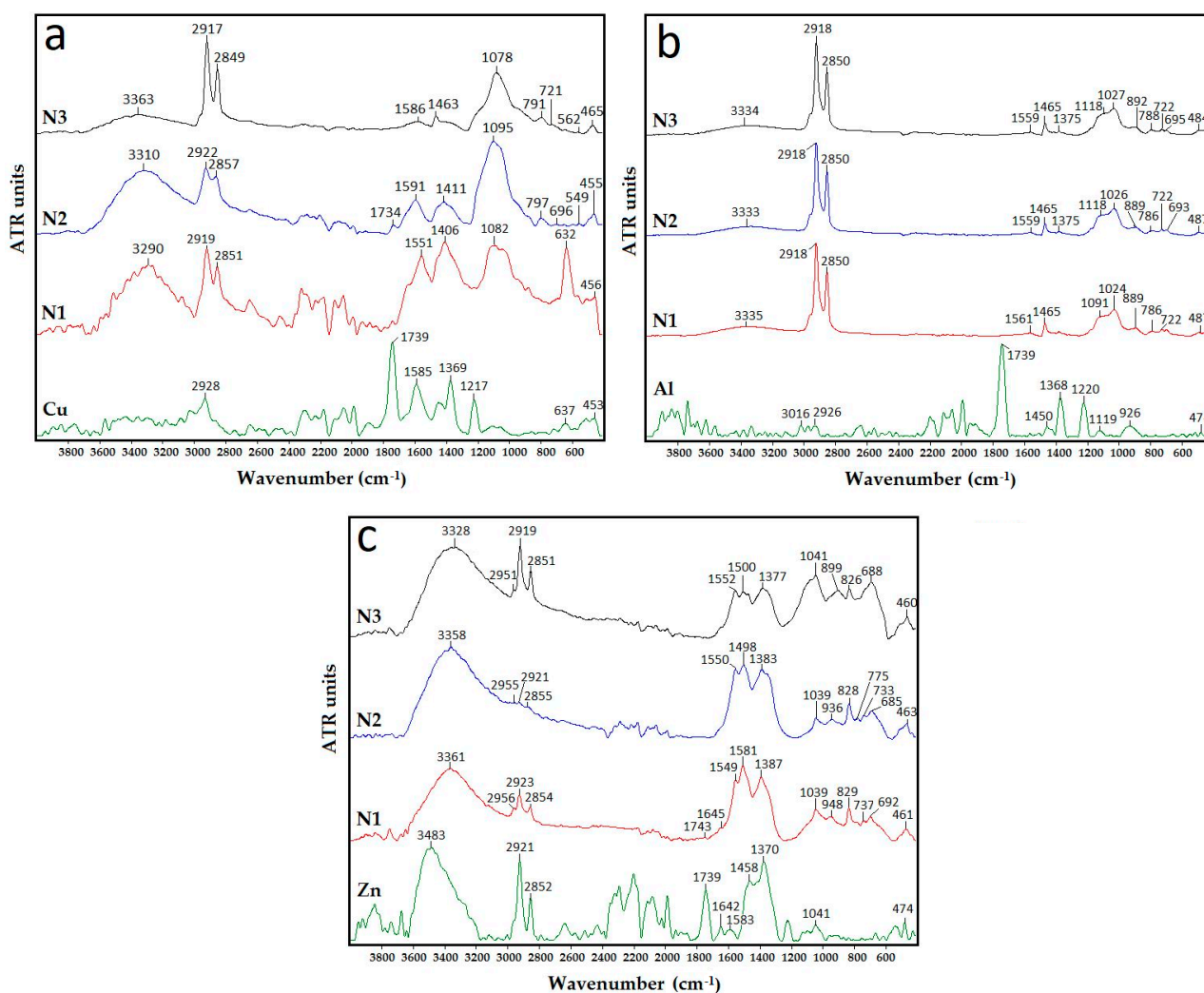


**Figure 3.** ATR-FTIR spectra of uncoated metallic substrates and of coated metallic substrates with ZnO-NPs modified with silane precursors (N1-TEOS/OTES, N2-TEOS/GPTMS, N3-TEOS/ODTES): (a) Cu, (b) Al and (c) Zn.

After deposition on metallic substrates (Al, Cu, Zn), the bonding structure of ZnO-NPs modified with silane precursors was analyzed by FTIR spectroscopy. Figure 3a–c shows broad IR absorption band between  $3300$  and  $3400\text{ cm}^{-1}$  which is characteristic of the O–H bending and O–H stretching vibrations, in the range of  $2956$ – $2851\text{ cm}^{-1}$  are the peaks for C–H stretching (symmetric and asymmetric) and the peaks in the range of  $1024$ – $1095\text{ cm}^{-1}$  are assigned to the Si–O–Si asymmetrical stretching vibrations confirming that the alkoxy-silanes molecules are covalently attached to the ZnO [36–40]. The peaks around  $899\text{ cm}^{-1}$  are related to symmetrical stretching mode of Zn–O–Si bonds, suggesting the successful covalent modification of ZnO-NPs surface by organosilanes. The disappearance of the shoulder at  $960\text{ cm}^{-1}$  due to free silanol hydroxide groups (Si–OH) confirms the introduction of the organofunctional groups onto the coated silica layers [23]. The peaks with

the moderated intensity observed in the range of 1370–1560  $\text{cm}^{-1}$  can be attributed to the functional groups C–O of asymmetric and symmetric stretching vibrations [3].

Sample N2, with GPTMS, on all metallic substrates, presents a peak at 693  $\text{cm}^{-1}$  which is assigned to the Si–O symmetric stretching vibration [41].

For all samples deposited on the metals, the peak presented in the range of 450–490  $\text{cm}^{-1}$ , helps to confirm the formation of the ZnO–Si bond [17,42]. The intensity of this peak is changed as a function of the type of metallic surface and this fact could be due to the vibration mode of zinc and oxygen bonds [43]. The incorporation of ZnO led to the appearance of a peak at 786  $\text{cm}^{-1}$  for Si–CH<sub>3</sub> [44].

It was observed that the intensity of the band situated at 3000–3400  $\text{cm}^{-1}$ , attributed to –OH groups, is changed as a function of the type of metallic surface and this fact can be due to the vibration mode of the –OH group on the surface of ZnO nanoparticles [45].

The cyclic component was observed at ~1083  $\text{cm}^{-1}$  in the case of the hybrid films deposited on the Cu surface (Figure 3a). For the hybrid films deposited on the Al surface (Figure 3b), the peak assigned to the Si–O stretch was observed at ~1025  $\text{cm}^{-1}$ . In the case of the hybrid films deposited on the Zn surface (Figure 3c), the peak of Si–O–Si is shifted to a wavenumber of ~1040  $\text{cm}^{-1}$  (asymmetric stretching vibration). If this peak is shifted to lower wavenumbers, there seems to be an overall decrease of the Si–O force constant due to the alkoxy silane group's incorporation. If the peak of Si–O–Si is shifted toward a higher wavenumber, this fact can be assigned to the presence of Si–C bonds (from the organofunctionalized co-precursors), which partially destroyed the symmetry of Si–O–Si linkages from silica hybrid network [46].

FTIR spectra revealed the influence of the silanic precursor upon the synthesized materials, depending on the length of the functional chain. These results indicated that the coated ZnO materials have been successfully grafted by organofunctional groups (glycidyl, octyl or octadecyl).

Literature data has shown that the shift of the Si–O–Si bond to longer wavelengths may be due to the increase of the intensity in the polymerization reaction of the Si–O–Si network by condensation of Si–OH groups.

### 3.4. Contact Angle Measurements

The wetting capacity of the coatings was determined through contact angle (CA) measurements, using water as liquid. CA is a measure of the adhesion between liquid drops (water) and solid surface. The final aim was to modify ZnO with silane functional groups to change the ZnO material surface from a hydrophilic to a hydrophobic nature.

Figure 4 shows the highest values of the contact angle (~144°) which were obtained for the coatings based on ZnO-TEOS/ODTES nanoparticles (N3). The ultrahydrophobic character can be explained by the presence of the octadecyl functionality from ODTES, combined with the obtained rough surfaces at nanometer level resulted after the incorporation of hydrophobically modified silica particles on the surface of the final hybrid film. The resulting surfaces exhibited significantly different wetting as a result of the nature of the end group (octyl, glycidyl, octadecyl). The increased hydrophobicity of the coatings from 96° to ~144° can be attributed to the more pronounced micro- to nanoparticle-textured surface with a refined roughness structure [47].

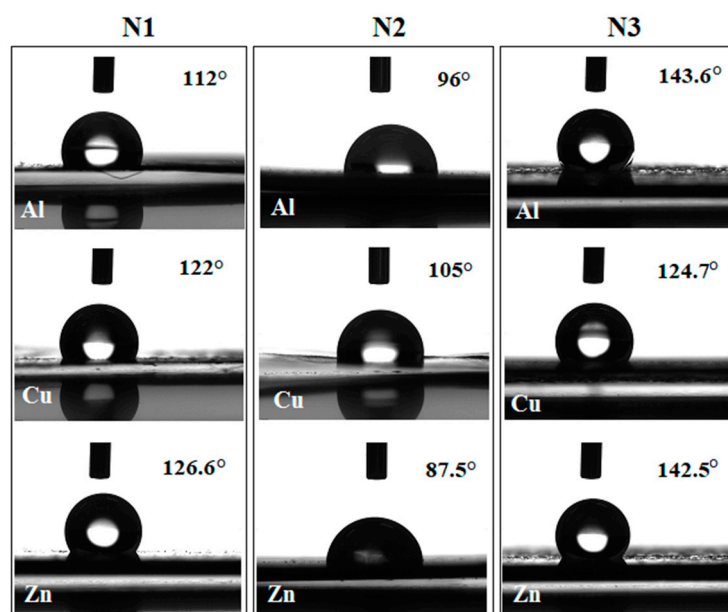


**Figure 4.** Values of water contact angles and profiles of water drop on metallic surfaces (Al, Cu, Zn) coated with sol-gel modified materials: N1 (ZnO-TEOS/OTES), N2 (ZnO-TEOS/GPTMS), N3 (ZnO-TEOS/ODTES).

The water contact angle values of coatings based on ZnO-TEOS/GPTMS nanoparticles (N2) deposited on Al and Cu were found to be around  $100^\circ$ . For coating deposited on Zn, the water contact angle was of  $\sim 88^\circ$ , which showed that the GPTMS formed a hydrophilic coating. This is probably due to the fact that epoxy does not fill the space between the ZnO nanoparticles. Compared to coating N2, it can be observed that coatings based on ZnO-TEOS/OTES nanoparticles (N1) indicate the high contact angles of  $\sim 122^\circ$ . The improvement in hydrophobicity might be due to the ZnO nanoparticles, which form air pockets between the water and the surface, leading to solid-liquid air interface that can impart surface roughness to the silica matrix. In the case of coatings based on ZnO-TEOS/ODTES nanoparticles (N3), the water contact angle values were of  $\sim 125^\circ$  and  $\sim 144^\circ$ , respectively. The hydroxyl groups of ODTES can react with hydroxyl groups on the surface of ZnO particles. ODTES plays a role as a “bridge” between ZnO particles. These “ODTES bridges” were formed by the dehydration between hydroxyl groups of ODTES and ZnO and thereby eliminating the defects which lead to ultrahydrophobicity [48]. The contact angle results confirmed that the silane precursors with long alkyl groups improve the formation of more compact siloxane networks [49].

### 3.5. Potentiodynamic Polarization Measurements

Corrosion resistance was determined by linear polarization technique. This technique consists of drawing linear polarization curves involving the following steps: measuring the open circuit potential ( $E_{oc}$ ) for a period of 1 h; plotting Tafel curves from  $-200$  (vs. OCP) to  $+200$  mV (vs. OCP), with a rate of scanning of  $1$  mV/s.

The Tafel curves corresponding to the coated metallic samples are shown in Figure 5 and the main corrosion parameters in Table 3.

From the corrosion tests performed in 3.5% NaCl solution, the following parameters were determined that characterize the corrosion resistance of the investigated samples: open circuit potential ( $E_{oc}$ ), corrosion potential ( $E_{corr}$ ), corrosion current density ( $i_{corr}$ ), slope of the cathodic curve ( $\beta_c$ ), slope of the anodic curve ( $\beta_a$ ).

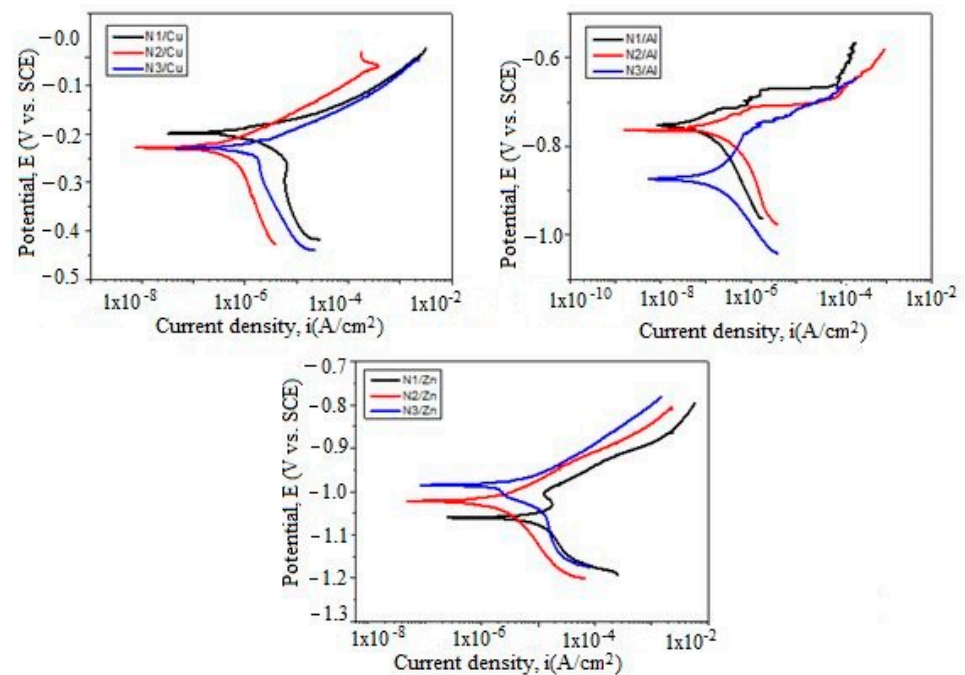


**Figure 5.** Tafel curves of metallic surfaces (Al, Cu, Zn) coated with sol-gel modified materials: N1 (ZnO-TEOS/OTES), N2 (ZnO-TEOS/GPTMS), N3 (ZnO-TEOS/ODTES).

**Table 3.** The main electrochemical parameters of the investigated samples.

Metallic Substrate	Sample	$E_{oc}$ (mV)	$E_{corr}$ (mV)	$i_{corr}$ (nA/cm <sup>2</sup> )	$\beta_c$ (mV)	$\beta_a$ (mV)	$R_p$ (k $\Omega$ cm <sup>2</sup> )
Cu	N1	-222	-197	2.397	274.25	47.37	7.32
	N2	-231	-227	812.97	370.30	74.61	33.21
	N3	-244	-229	1.935	343.13	56.79	10.94
Al	N1	-764	-755	109.66	166.60	65.84	187.10
	N2	-779	-757	130.31	145.25	37.31	99.05
	N3	-844	-871	155.26	124.94	115.75	168.26
Zn	N1	-996	-1.059	5.013	97.72	95.82	4.19
	N2	-1.005	-1.021	2.380	156.01	70.15	8.84
	N3	-981	-985	5.710	242.58	80.90	4.61

#### Polarization Resistance ( $R_p$ )

The polarization resistance ( $R_p$ ) of the specimens was determined by linear polarization method (LPR) as the slope neared the potential after the steady state is reached [50].

By analyzing the main electrochemical parameters' values it can be observed that, among the coatings achieved on the Cu substrate, the smallest corrosion current density ( $i_{corr}$ ), with a value of 812.97 nA/cm<sup>2</sup>, was noted for the N2, thus demonstrating a better electrochemical behavior. The N1 coatings on the Al substrate demonstrated better electrochemical behavior, having the smallest  $i_{corr}$  value (109.66 nA/cm<sup>2</sup>), while in the case of the coatings on the Zn substrate, the N2 was highlighted (2.380 nA/cm<sup>2</sup>).

Regarding the polarization resistance, the highest values (and thus an enhanced electrochemical behavior) were obtained for the same coatings that had the smallest corrosion current density with respect to the substrate material (N2 for the Cu substrate, N1 for the Al substrate and N2 for the substrate). Though, it can be noticed that the evolution of polarization resistance is similar only for the coatings on the Cu and Zn substrates. Thus, the value increases for N2 and decreases for N3, taking as a reference the value of N1. In

the case of Al used as substrate, the evolution is different, meaning that it is the opposite from that obtained for Cu and Zn.

Moreover, by comparing the anticorrosive efficiency of the coatings, regardless which substrate material was used, it can be observed that the proposed coatings, N1, N2 and N3, respectively, showed better values when used to coat the Al substrate.

### 3.6. Films Thickness and Roughness Measurements

Thickness and roughness of the ZnO-based surface coatings (N1 (ZnO-TEOS/OTES), N2 (ZnO-TEOS/GPTMS), N3 (ZnO-TEOS/ODTES)) deposited on the metallic surfaces (Al, Cu, Zn) are shown in Figure 6.

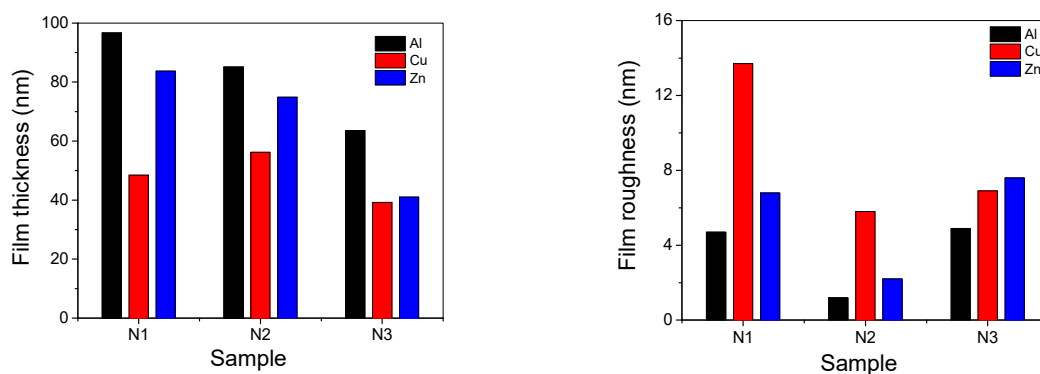


**Figure 6.** Thickness and roughness of the ZnO-based surface coatings N1 (ZnO-TEOS/OTES), N2 (ZnO-TEOS/GPTMS) and N3 (ZnO-TEOS/ODTES), deposited on the metallic surfaces (Al, Cu, Zn), determined by the ellipsometric measurements.

A decreasing tendency of the thickness may be observed, following the organic groups order  $N1 > N2 > N3$  for the samples deposited on Al and Zn substrates, showing the influence of the precursors on the sample thickness. However, for the samples deposited on Cu there is a slight thickness increase from N1 to N2, followed by its further decrease for the N3 sample. Within the same organic groups, the influence of the substrate is clearly observed, the thickness following the decreasing tendency in the series  $Al > Zn > Cu$ .

The roughness values were found to be in the range of 1.2–13.7 nm, as shown in the Figure 6. The lowest roughness values are observed for the sample N2 for all three substrates, although the differences are no larger than a few nanometers. The highest roughness value was obtained for the N1 sample deposited on Cu.

## 4. Conclusions

The zinc oxide nanomaterials modified with different silane coupling agents (octyltriethoxysilane (OTES), octadecyltriethoxysilane (ODTES) and (3-glycidioxypropyl) trimethoxysilane (GPTMS)) were synthesized via sol-gel process. Coatings with ultrahydrophobic properties and anti-corrosive effects were prepared using various metallic substrates (aluminum, copper and zinc).

The ESEM images of the topographic surface clearly indicate the aggregation of the particles, with different nanoparticle sizes (corroborated with DLS analyses) depending on the length of the alkyl functional groups of the silanic precursors.

FTIR spectra indicated that the coated ZnO materials have been successfully grafted by organofunctional groups (glycidioxy, octyl or octadecyl).

In this study, water contact angles were increased to nearly  $145^\circ$  by ZnO-TEOS/ODTES nanostructures deposited on metallic substrates.

Based on electrochemical results, one can conclude that the N2 (ZnO-TEOS/GPTMS) sample gives the best results regarding corrosion and the best electrochemical behavior when deposited on Al substrate.

Owing to the good performance in a corrosive environment and to the ultrahydrophobic properties, modified ZnO coatings can be highly suitable for industrial applications.

**Author Contributions:** Conceptualization, R.S. and V.P.; methodology, R.S. and V.P.; formal analysis, C.M.N., E.A., C.M.C., H.S. and I.C.G.; writing—original draft preparation, R.S. and V.P.; funding acquisition, F.O. All authors have read and agreed to the published version of the manuscript.

**Funding:** This research was funded by Ministry of Research and Innovation, Nucleu Programme, grant number P.N.19.23.01.01 Smart-Bi” and “by a grant from the Romanian Ministry of Education and Research, CNCS-UEFISCDI, project number PN-III-P1-1.1-TE-2019-2053, within PNCDI III.

**Institutional Review Board Statement:** Not applicable.

**Informed Consent Statement:** Not applicable.

**Data Availability Statement:** The data are not publicly available due to their containing information that could compromise the privacy of research participants.

**Acknowledgments:** The author would like to thank to Eng. Simona Caprarescu, who procured and donated the metallic surfaces.

**Conflicts of Interest:** The authors declare no conflict of interest. The funders had no role in the design of the study; in the collection, analyses, or interpretation of data; in the writing of the manuscript, or in the decision to publish the results.

## References

1. Faizan, M.; Hayat, S.; Pichtel, J. Effects of zinc oxide nanoparticles on crop plants: A perspective analysis. In *Sustainable Agriculture Reviews 41*; Springer: Berlin/Heidelberg, Germany, 2020; pp. 83–99.
2. Czyżowska, A.; Barbasz, A. A review: Zinc oxide nanoparticles—Friends or enemies? *Int. J. Environ. Health Res.* **2020**, 1–17. [[CrossRef](#)] [[PubMed](#)]
3. Aboorvakani, R.; Kennady Vethanathan, S.J.; Madhu, K.U. Influence of zn concentration on zinc oxide nanoparticles and their anti-corrosion property. *J. Alloys Compd.* **2020**, 834, 155078. [[CrossRef](#)]
4. Rivero, P.J.; Maeztu, J.D.; Berlanga, C.; Miguel, A.; Palacio, J.F.; Rodriguez, R. Hydrophobic and corrosion behavior of sol-gel hybrid coatings based on the combination of TiO<sub>2</sub> nps and fluorinated chains for aluminum alloys protection. *Metals* **2018**, 8, 1076. [[CrossRef](#)]
5. Rashvand, M.; Ranjbar, Z. Effect of nano-zno particles on the corrosion resistance of polyurethane-based waterborne coatings immersed in sodium chloride solution via eis technique. *Prog. Org. Coat.* **2013**, 76, 1413–1417. [[CrossRef](#)]
6. Ramezanzadeh, B.; Attar, M.M. Studying the effects of micro and nano sized zno particles on the corrosion resistance and deterioration behavior of an epoxy-polyamide coating on hot-dip galvanized steel. *Prog. Org. Coat.* **2011**, 71, 314–328. [[CrossRef](#)]
7. Fayomi, O.S. Effect of composite particulate reinforcement on the morphology, anti-corrosion and hardness properties of fabricated zn-zno coatings. *J. Mater. Environ. Sci.* **2015**, 6, 963–968.
8. Zhang, D.; Wang, L.; Qian, H.; Li, X. Superhydrophobic surfaces for corrosion protection: A review of recent progresses and future directions. *J. Coat. Technol. Res.* **2016**, 13, 11–29. [[CrossRef](#)]
9. Figueira, R.B.; Fontinha, I.R.; Silva, C.J.R.; Pereira, E.V. Hybrid sol-gel coatings: Smart and green materials for corrosion mitigation. *Coatings* **2016**, 6, 12. [[CrossRef](#)]
10. Mohamed, A.M.A.; Abdullah, A.M.; Younan, N.A. Corrosion behavior of superhydrophobic surfaces: A review. *Arab. J. Chem.* **2015**, 8, 749–765. [[CrossRef](#)]
11. Ma, M.; Hill, R.M. Superhydrophobic surfaces. *Curr. Opin. Colloid Interface Sci.* **2006**, 11, 193–202. [[CrossRef](#)]
12. Ou, J.F.; Liu, M.Z.; Li, W.; Wang, F.J.; Xue, M.S.; Li, C.Q. Corrosion behavior of superhydrophobic surfaces of ti alloys in nacl solutions. *Appl. Surf. Sci.* **2012**, 258, 4724–4728. [[CrossRef](#)]
13. Yin, Y.; Liu, T.; Chen, S.; Liu, T.; Cheng, S. Structure stability and corrosion inhibition of super-hydrophobic film on aluminum in seawater. *Appl. Surf. Sci.* **2008**, 255, 2978–2984. [[CrossRef](#)]
14. Montemor, M.F. Functional and smart coatings for corrosion protection: A review of recent advances. *Surf. Coat. Technol.* **2014**, 258, 17–37. [[CrossRef](#)]
15. Longhi, M.; Kunsta, S.R.; Beltrami, L.V.R.; Kerstner, E.K.; Silva Filho, C.I.; Sarmiento, V.H.V.; Malfatti, C. Effect of tetraethoxy-silane (teos) amounts on the corrosion prevention properties of siloxane-pmma hybrid coatings on galvanized steel substrates. *Mater. Res.* **2015**, 18, 1140–1155. [[CrossRef](#)]
16. Foo, K.L.; Hashim, U.; Muhammad, K.; Voon, C.H. Sol-gel synthesized zinc oxide nanorods and their structural and optical investigation for optoelectronic application. *Nanoscale Res. Lett.* **2014**, 9, 429. [[CrossRef](#)] [[PubMed](#)]
17. Jurablu, S.; Farahmandjou, M.; Firoozabadi, T.P. Sol-gel synthesis of zinc oxide (zno) nanoparticles: Study of structural and optical properties. *J. Sci. Islamic Repub. Iran* **2015**, 26, 281–285.
18. Heakal, F.E.-T.; Elkholy, A.E. Gemini surfactants as corrosion inhibitors for carbon steel. *J. Mol. Liquids* **2017**, 230, 395–407. [[CrossRef](#)]
19. Qian, Y.; Li, Y.; Jungwirth, S.; Seely, N.; Fang, Y.; Shi, X. The application of anti-corrosion coating for preserving the value of equipment asset in chloride-laden environments: A. *Int. J. Electrochem. Sci* **2015**, 10, 10756–10780.

20. Verma, C.; Ebenso, E.E.; Quraishi, M.A. Ionic liquids as green and sustainable corrosion inhibitors for metals and alloys: An overview. *J. Mol. Liquids* **2017**, *233*, 403–414. [[CrossRef](#)]
21. El Hamdani, N.; Fdil, R.; Tourabi, M.; Jama, C.; Bentiss, F. Alkaloids extract of retama monosperma (l.) boiss. Seeds used as novel eco-friendly inhibitor for carbon steel corrosion in 1m hcl solution: Electrochemical and surface studies. *Appl. Surf. Sci.* **2015**, *357*, 1294–1305. [[CrossRef](#)]
22. Al-Dahiri, R.H.; Turkustani, A.M.; Salam, M.A. The application of zinc oxide nanoparticles as an eco-friendly inhibitor for steel in acidic solution. *Int. J. Electrochem. Sci* **2020**, *15*, 442–457. [[CrossRef](#)]
23. El-Nahhal, I.M.; Salem, J.K.; Kuhn, S.; Hammad, T.; Hempelmann, R.; Al Bhaisi, S. Synthesis & characterization of silica coated and functionalized silica coated zinc oxide nanomaterials. *Powder Technol.* **2016**, *287*, 439–446.
24. Laurenti, M.; Stassi, S.; Canavese, G.; Cauda, V. Surface engineering of nanostructured zno surfaces. *Adv. Mater. Interfaces* **2017**, *4*, 1600758. [[CrossRef](#)]
25. Topala, P.; Ojegov, A.; Besliu, V. Formation of anticorrosive structures and thin films on metal surfaces by applying edm. In *Corrosion Inhibitors*; IntechOpen: London, UK, 2019.
26. Mirhashemihaghighi, S.; Światowska, J.; Maurice, V.; Seyeux, A.; Zanna, S.; Salmi, E.; Ritala, M.; Marcus, P. Corrosion protection of aluminium by ultra-thin atomic layer deposited alumina coatings. *Corros. Sci.* **2016**, *106*, 16–24. [[CrossRef](#)]
27. Krishnan, M.A.; Aneja, K.S.; Shaikh, A.; Bohm, S.; Sarkar, K.; Bohm, H.L.M.; Raja, V.S. Graphene-based anticorrosive coatings for copper. *RSC Adv.* **2018**, *8*, 499–507. [[CrossRef](#)]
28. Lapeire, L.; Lombardia, E.M.; De Graeve, I.; Terry, H.; Verbeken, K. Influence of grain size on the electrochemical behavior of pure copper. *J. Mater. Sci.* **2017**, *52*, 1501–1510. [[CrossRef](#)]
29. Prosek, T.; Hagström, J.; Persson, D.; Fuertes, N.; Lindberg, F.; Chocholatý, O.; Taxén, C.; Šerák, J.; Thierry, D. Effect of the microstructure of zn-al and zn-al-mg model alloys on corrosion stability. *Corros. Sci.* **2016**, *110*, 71–81. [[CrossRef](#)]
30. Goo, B.J.; Lee, B.R.; Moon, M.B.; Oh, S.J. Corrosion properties of Zn alloy coated steel sheet for automotive panels. In Proceedings of the 19th International Corrosion Congress, Jeju, Korea, 2–6 November 2014.
31. Prosek, T.; Nazarov, A.; Le Gac, A.; Thierry, D. Coil-coated zn–mg and zn–al–mg: Effect of climatic parameters on the corrosion at cut edges. *Prog. Org. Coat.* **2015**, *83*, 26–35. [[CrossRef](#)]
32. Alwan, R.M.; Kadhim, Q.A.; Sahan, K.M.; Ali, R.A.; Mahdi, R.J.; Kassim, N.A.; Jassim, A.N. Synthesis of zinc oxide nanoparticles via sol–gel route and their characterization. *Nanosci. Nanotechnol.* **2015**, *5*, 1–6.
33. Vasconcelos, D.C.L.; Nunes, E.H.M.; Vasconcelos, W.L. Aes and ftir characterization of sol–gel alumina films. *J. Non-Crystalline Solids* **2012**, *358*, 1374–1379. [[CrossRef](#)]
34. Betancourt-Galindo, R.; Reyes-Rodríguez, P.Y.; Puente-Urbina, B.A.; Avila-Orta, C.A.; Rodríguez-Fernández, O.S.; Cadenas-Pliego, G.; Lira-Saldivar, R.H.; García-Cerda, L.A. Synthesis of copper nanoparticles by thermal decomposition and their antimicrobial properties. *J. Nanomater.* **2014**, *2014*, 980545. [[CrossRef](#)]
35. Włodarski, M.; Putkonen, M.; Norek, M. Infrared absorption study of zn–s hybrid and zns ultrathin films deposited on porous aao ceramic support. *Coatings* **2020**, *10*, 459. [[CrossRef](#)]
36. Purcar, V.; Șomoghi, R.; Nițu, S.G.; Nicolae, C.-A.; Alexandrescu, E.; Gifu, I.C.; Gabor, A.R.; Stroescu, H.; Ianchiș, R.; Căprărescu, S.; et al. The effect of different coupling agents on nano-zno materials obtained via the sol-gel process. *Nanomaterials* **2017**, *7*, 439. [[CrossRef](#)]
37. Álvarez, D.; Collazo, A.; Nóvoa, X.R.; Pérez, C. Assessment of zno nanoparticles as anticorrosive pigment in hybrid sol–gel films. *Prog. Org. Coat.* **2016**, *96*, 3–12. [[CrossRef](#)]
38. Ghosh, S.P. Synthesis and Characterization of Zinc Oxide Nanoparticles by Sol-Gel Process. Master’s Thesis, National Institute of Technology, Orissa, India, 2012.
39. El Saeed, A.M.; Abd El-Fattah, M.; Azzam, A.M. Synthesis of zno nanoparticles and studying its influence on the antimicrobial, anticorrosion and mechanical behavior of polyurethane composite for surface coating. *Dyes Pigment.* **2015**, *121*, 282–289. [[CrossRef](#)]
40. Rissi, N.C.; Hammer, P.; Chiavacci, L.A. Surface modification of zno quantum dots by organosilanes and oleic acid with enhanced luminescence for potential biological application. *Mater. Res. Express* **2017**, *4*, 015027. [[CrossRef](#)]
41. Gopal, N.O.; Narasimhulu, K.V.; Rao, J.L. Epr, optical, infrared and raman spectral studies of actinolite mineral. *Spectrochim. Acta Part A Mol. Biomol. Spectrosc.* **2004**, *60*, 2441–2448. [[CrossRef](#)] [[PubMed](#)]
42. Jiang, M.-Y.; Wu, L.-K.; Hu, J.-M.; Zhang, J.-Q. Silane-incorporated epoxy coatings on aluminum alloy (aa2024). Part 1: Improved corrosion performance. *Corros. Sci.* **2015**, *92*, 118–126. [[CrossRef](#)]
43. Mallakpour, S.; Madani, M. Use of silane coupling agent for surface modification of zinc oxide as inorganic filler and preparation of poly(amide-imide)/zinc oxide nanocomposite containing phenylalanine moieties. *Bull. Mater. Sci.* **2012**, *35*, 333–339. [[CrossRef](#)]
44. Nikolic, G.; Zlatkovic, S.; Cakic, M.; Cakic, S.; Lacnjevac, C.; Rajic, Z. Fast fourier transform ir characterization of epoxy gy systems crosslinked with aliphatic and cycloaliphatic eh polyamine adducts. *Sensors* **2010**, *10*, 684–696. [[CrossRef](#)]
45. Tinio, J.V.G.; Simfroso, K.T.; Peguit, A.D.M.V.; Candidato, R.T. Influence of oh<sup>-</sup> ion concentration on the surface morphology of Zno-SiO<sub>2</sub> nanostructure. *J. Nanotechnol.* **2015**, *2015*, 686021. [[CrossRef](#)]
46. Petcu, C.; Nistor, C.L.; Purcar, V.; Cintează, L.O.; Spătaru, C.-I.; Ghiurea, M.; Ianchiș, R.; Anastasescu, M.; Stoica, M. Facile preparation in two steps of highly hydrophobic coatings on polypropylene surface. *Appl. Surf. Sci.* **2015**, *347*, 359–367. [[CrossRef](#)]

47. Conradi, M.; Kocijan, A. Comparison of the surface and anticorrosion properties of SiO<sub>2</sub> and TiO<sub>2</sub> nanoparticle epoxy coatings. *Mater. Teh.* **2017**, *51*, 1043–1046. [[CrossRef](#)]
48. Chakradhar, R.P.S.; Kumar, V.D.; Rao, J.L.; Basu, B.J. Fabrication of superhydrophobic surfaces based on zno–pdms nanocomposite coatings and study of its wetting behaviour. *Appl. Surf. Sci.* **2011**, *257*, 8569–8575. [[CrossRef](#)]
49. Orтели, S.; Costa, A.L. Insulating thermal and water-resistant hybrid coating for fabrics. *Coatings* **2020**, *10*, 72. [[CrossRef](#)]
50. Dinu, M.; Hauffman, T.; Cordioli, C.; Vladescu, A.; Braic, M.; Hubin, A.; Cotrut, C.M. Protective performance of zr and cr based silico-oxynitrides used for dental applications by means of potentiodynamic polarization and odd random phase multisine electrochemical impedance spectroscopy. *Corros. Sci.* **2017**, *115*, 118–128. [[CrossRef](#)]